Paull, C.K., Matsumoto, R., Wallace, P.J., and Dillon, W.P. (Eds.), 2000
Proceedings of the Ocean Drilling Program, Scientific Results, Vol. 164

27. IN SITU MEASUREMENTS OF *P*-WAVE ATTENUATION IN THE METHANE HYDRATE– AND GAS-BEARING SEDIMENTS OF THE BLAKE RIDGE[1]

Warren T. Wood,[2] W. Steven Holbrook,[3] and Hartley Hoskins[4]

ABSTRACT

Recent drilling on the crest of the Blake Ridge during Ocean Drilling Program Leg 164 has provided an opportunity to compare estimates of attenuation from seismic data with direct samples of hydrate and gas in this region with the objective of using attenuation to remotely quantify hydrate and gas. Hydrate formation at the sediment grain contacts rather than in the pore spaces may significantly decrease the seismic attenuation. Because attenuation may be estimated from single-channel data, it would be more useful in hydrate detection than velocity, which requires more expensive multichannel data. In this analysis both single-channel seismic data and vertical seismic profile (VSP) data were inverted using a spectral modeling technique. For the single-channel data, this was performed using a simulated annealing algorithm, and for VSP data, the model updates were implemented manually. The results from both independent data sets are consistent with each other in each of the hydrate- and gas-stability zones. Values of the quality factor Q for hydrate-bearing sediments fall within the range expected of nonhydrate-bearing, fine-grained marine sediments, ranging from ~90 to 600, suggesting that small amounts of hydrate do not significantly affect Q. All values of Q less than ~90 were associated with gassy sediments; some were as low as $Q = 6$. Q within the hydrate-stability field changes systematically, reaching a minimum directly below the ridge crest. As expected, Q in the gassy sediments appears to correlate inversely with reflection strength.

INTRODUCTION

Background

Methane in deep-sea sediments can take the form of a solid hydrate as well as free gas, two forms with physical properties significantly different from each other as well as from the fine-grained muds of the Blake Ridge in which the hydrate is found (Fig. 1). For this reason we are able to quantify the presence of methane through seismic methods, namely through the measurement of acoustic or compressional velocity (V_p), shear velocity (V_s), and quality factor (Q) or inverse of effective attenuation. Measurements of V_p in the hydrate stability zone (HSZ), and underlying gas stability zone (GSZ) of the Blake Ridge have been made using multichannel seismic reflection data (Paull and Dillon, 1981; Rowe and Gettrust, 1993; Wood et al. 1994), wide-angle, ocean-bottom hydrophone data (Katzman et al., 1994; Korenaga et al., 1997), and most recently vertical seismic profiles (VSPs) acquired on Ocean Drilling Program (ODP) Leg 164 (Holbrook et al., 1996; Pecher et al., 1997, and unpubl. data). Although V_p is quite useful for delineating the regions of gas below the HSZ, only moderate success has been achieved at quantifying small amounts of hydrate within the HSZ, (Holbrook et al., 1996). If the hydrate acts as a cement (Dvorkin and Nur, 1993), then V_s and Q may be quite sensitive to small amounts of hydrate. Pecher et al. (1997) have reported an intriguing high V_s layer in the HSZ, but to date thorough analyses for Q in this area have not been widely reported.

We used two independent data sets in this study, a single-channel seismic (SCS) reflection profile acquired as part of a site survey for Leg 164 (Line 31, Katzman et al., 1994), which passes over Sites 994, 995, and 997, and vertical seismic profiles acquired with air- and water-gun sources at Site 995. The SCS source was a 160-in^3 dual

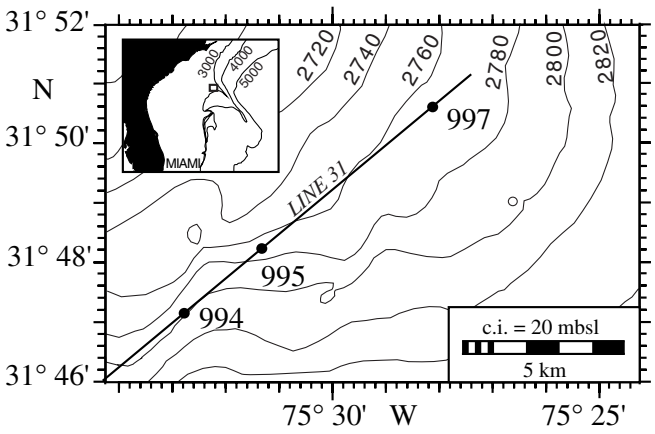

Figure 1. Three vertical seismic profiles (at ODP Sites 994, 995, and 997) were acquired at sites that lie along the transect of a high-resolution, surface-towed, single-channel line acquired by a dual-chamber air gun, (Line 31). The transect crosses the crest of the Blake Ridge, where gas and fluids may be expected to accumulate.

chamber air-gun, with minimal bubble pulse and a wide band (20–150 Hz at 20 dB down from the peak). The VSPs on Leg 164 were acquired with a 300-in^3 Bolt model PAR 1500 air-gun, suspended 5 m from the sea surface, and a 400-in^3 Seismic Systems model P400 pneumatic water-gun suspended 4 m from the sea surface. The source signatures and spectra are shown in Figure 2, revealing the compact broad band nature of the air-gun source used in the SCS profile.

The SCS line analyzed, Line 31 from Katzman et al. (1994), is displayed in Figure 3A after application of a time shift to make the seafloor horizontal. An alternative means of displaying the data is to plot at each time sample a frequency that is representative of the amplitude spectrum for a portion of the trace windowed about that sample. The representative frequency used here is the centroid frequency. This is computed by first determining the area of the frequency domain amplitude spectrum for the windowed portion that lies above the noise. The noise level for this calculation was assumed to be 0.1

[1]Paull, C.K., Matsumoto, R., Wallace, P.J., and Dillon, W.P. (Eds.), 2000. *Proc. ODP, Sci. Results,* 164: College Station, TX (Ocean Drilling Program).
[2]Naval Research Laboratory, Code 7432 Stennis Space Center, MS 39529, U.S.A. warren.wood@nrlssc.navy.mil
[3]Univ. of Wyoming, P.O. Box 3006, Laramie, WY 82071, U.S.A.
[4]Woods Hole Oceanographic Institute, Woods Hole, MA 02543, U.S.A.

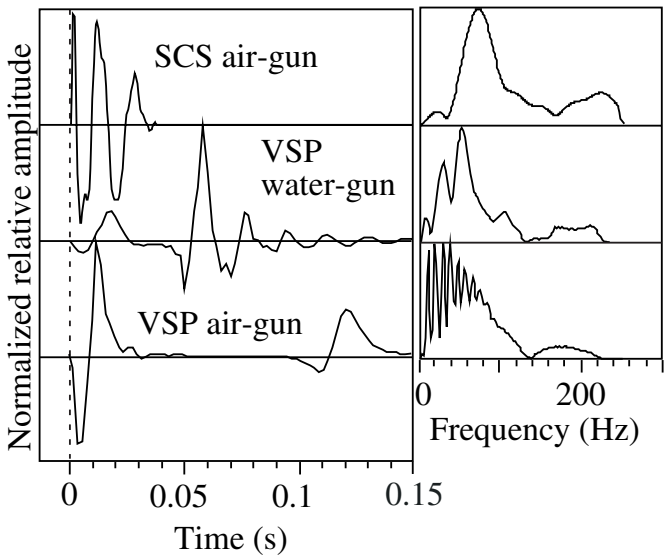

Figure 2. The three source functions of the data used in the attenuation analysis and their corresponding amplitude spectra are shown. The VSP air-gun, and water-gun signatures were taken from direct water-wave arrivals at a monitor hydrophone. The SCS air-gun signature was inverted from the seismic data using the technique of W.T. Wood (unpubl. data). None of the amplitudes are expressed as log ratio values.

of the peak value, or 20 dB down. The centroid frequency is that frequency which divides the area of the amplitude spectrum above the noise into two equal area portions. The result of this operation is the spectrogram shown in Figure 3B. Because migration can distort frequency spectra, the spectrogram was computed using unmigrated data. The time window used to compute the frequencies was a 64 sample cosine tapered window. To laterally smooth the result, the spectra from four adjacent traces were stacked before centroid frequency computation. It is quite apparent from this display that the data are sensitive to frequency content (note the sharp drop below the BSR), and that a quantitative analysis of this effect may at least allow detection, and possibly quantification, of hydrate and gas. With this objective, a nonlinear inversion for attenuation based on spectral modeling was applied to the data.

Defining *Q*

To implement the inversion, we use the operational definition of attenuation given by Aki and Richards, (1980),

$$A(t) = A_o\,[1 - \pi ft/Qn]^n, \qquad (1)$$

where $A(t)$ is the amplitude of the seismic signal of frequency f, after traveling for a length of time t, and number of cycles n, through a medium with a quality factor of Q, and with a starting amplitude $A_o = [A(t = 0)]$. Note that Q and attenuation are inversely related. Because we may want to analyze layers that are less than a few cycles thick, we retain this exact form of the equation above in favor of the more common approximate form for many cycles, which involves an exponential (Aki and Richards, 1980).

Mechanisms for intrinsic Q (absorption) include grain sliding, viscous flow of pore fluid (or gas), and perhaps viscous relaxation (Stoll and Bryan, 1970; Johnston et al., 1979). Another phenomenon, scattering, as from intrabed multiples, has nearly the same effect as intrinsic Q and can be included with the intrinsic Q into an inclusive effective Q. Schoenberger and Levin (1974, 1978) and Kang and McMechan (1994) have found independently that 20%–80% of the effective attenuation may be attributable to either phenomenon, depending on the geological model. In this study we measure effective Q, so both mechanisms must be included in the interpretation of the results. We also assume here that Q is frequency independent (implying a dispersionless medium), which is a reasonable assumption at these frequencies (Murphy, 1982; Bowles, 1997).

Attenuation in Fine-Grained Sediments

To determine the magnitude of a possible Q anomaly due to hydrate or gas, we must first determine what Q should be expected from hydrate-free sediments. Although the bulk of field and lab studies reported in the geophysics literature regarding attenuation have been performed on sands, Bowles (1997) recently compiled an extensive list of compressional wave attenuation studies that have been performed on fully saturated fine-grained marine sediments. The results were originally reported in units of dB/m and were converted to Q for comparison here using a velocity of 1600 m/s. For frequencies between 20 and 250 Hz, reported Q for the silts and clays covered a very large range, from 60 to 2500. Most of the values are concentrated between 200 and 700. These values are similar to Q values obtained through analysis of VSP data in Texas by Hauge (1981), who reported Q as high as ~500 for shales in the Gulf of Mexico. There does not seem to be a significant modal character to the data (suggesting different attenuations for hydrate-bearing sediment), nor was the presence of hydrate reported. We therefore assume a reasonable Q for nonhydrate-bearing sediment to be ~400.

There exist very few quantitative reports of Q in gas sands, and even fewer in gassy mud. Some of the lowest Q values reported for fine-grained marine sediments (Q = 50–60; Hamilton, 1976; Bowles, 1997) may have unknowingly incorporated some gas, but they were not reported as gas bearing. Using sandstones, Murphy (1982) measured Q over a range of partial saturations and frequencies, and showed at 100 Hz a decrease in Q from 50 at 100% saturation to 22 at 90% saturation and back to 50 as saturation decreases. This rather interesting local minimum of Q at partial saturation was attributed to peak loss of energy from pore fluids moving relative to the surrounding matrix. Others report similar values (Q ranging between 10 and 100) for dry, as well as saturated sandstones in the lab (Toksoz et al., 1979; Frisillo and Stewart, 1980) and unconsolidated sediments in the field (Badri and Mooney, 1987). We therefore expect Q for gassy muds to be between 10 and 100.

For hydrate-bearing sediments, we expect a higher Q than for hydrate-free sediments, analogous to frozen vs. unfrozen sediments, (Toksoz et al., 1979). Perhaps the best estimate of Q through hydrate-bearing sediment comes from Brienzo (1992), who made no mention of hydrate, but reported somewhat high values of Q, ranging from 660 at the seafloor to 175 at 750 mbsf in the Monterey deep-sea fan, a thick sediment column in 2800 m of water where hydrates are very likely to be found. This value is consistent with the higher Q values reported by Bowles (1997), which may also have been unknowingly acquired in hydrate-bearing sediments. Although Jacobson et al. (1981) also reports Q from deep water (~3000 m in the Bay of Bengal), the values are generally between 50 and 200. Based on these reports, our a priori estimates of Q are 200–700 in the HSZ and Q = 10–100 in the GSZ.

METHOD OF ANALYSIS

In Situ Measurement of *Q*

Because the attenuation as given by Equation 1 is based on energy loss per oscillation and for a given traveltime, the high frequencies undergo more oscillations than do the low frequencies, the higher frequencies are preferentially attenuated, and wavelet shape changes

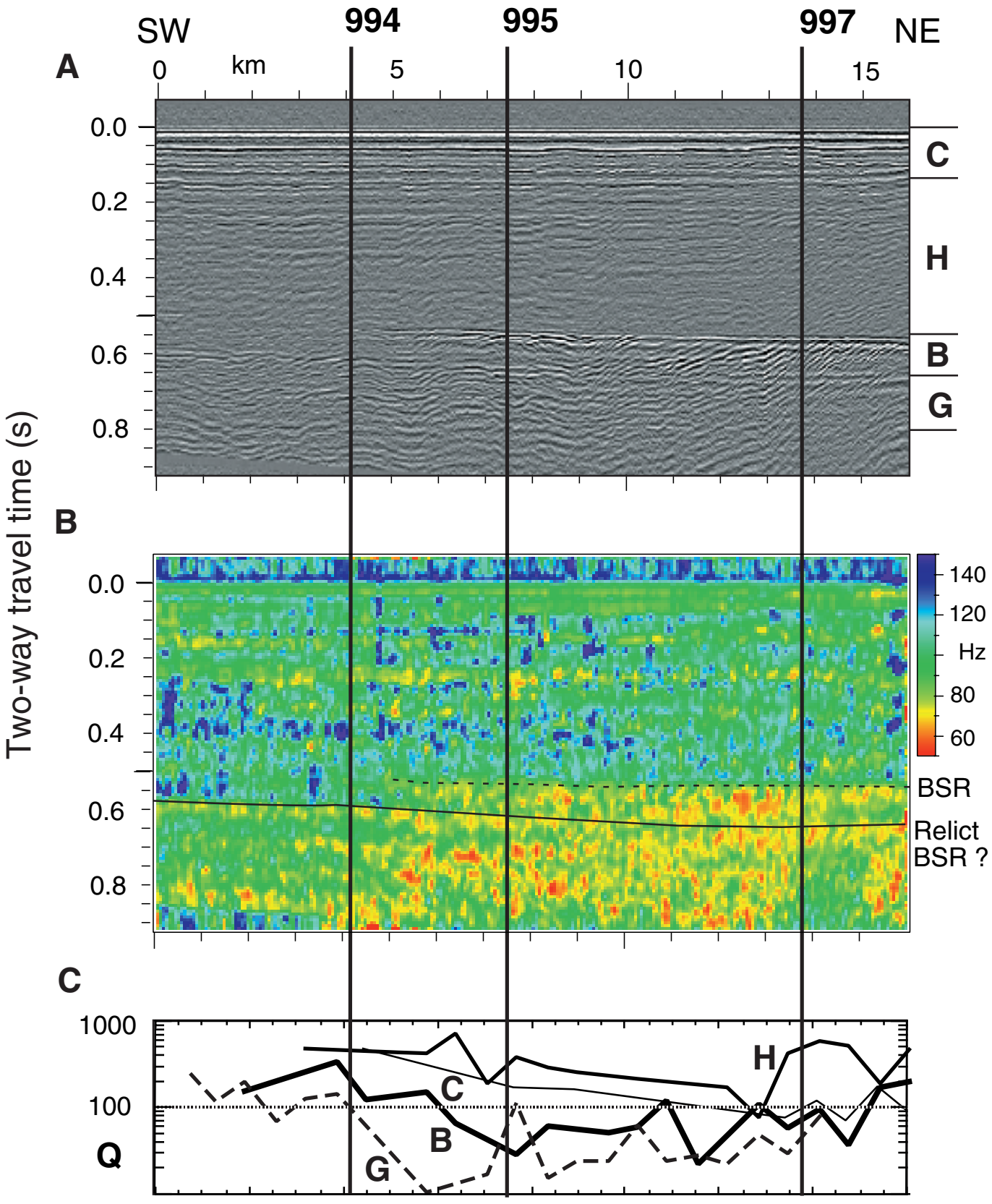

Figure 3. **A.** Line 31, which passes over the crest of the Blake Ridge, was time shifted to make the water-bottom horizontal. **B.** A sliding spectrum applied to this line reveals a sharp drop in frequency at the BSR and another gas-charged layer (possibly a relict BSR), each of which represents the top of gas. **C.** Inversion for quality factor *Q* shows the highest values for layer H where the hydrate was found.

with time. There are a variety of techniques by which Q can be measured from field seismic data, all based on this phenomenon. For a source wavelet that is symmetric in time the peak frequency is also the centroid frequency, and the instantaneous frequency from complex analysis may be used (LeBlanc et al., 1991; Panda et al., 1994). Other methods include rise-time analysis (Tarif and Bourbie, 1987), spectral ratios (Jacobson et al., 1981), inverse Q filtering (Gelius, 1987), and wavelet modeling in the time or frequency domain (Jannsen et al., 1985).

A significant obstacle in modeling Q using any of these methods is the interference between layers that are separated by less than a pulse length in arrival time. This interference produces a composite signal with a frequency content lower than that of the individual contributing signals. The magnitude of this effect depends on the relative reflection strengths and layer thicknesses and is in general unpredictable. To mitigate this effect, we analyze data over a range of time and space (0.064 s and 20 traces). A large range will increase the stability and accuracy of the inversion at the expense of resolution. We assume that in the particular case of the very homogenous sediments of the Blake Ridge, the sedimentary structure, and therefore the interference, is consistent from window to window. The interference will affect absolute frequency content, but relative changes may still be accurately observed.

Spectral Modeling

The method we chose to invert for Q here is that of spectral modeling, similar to that of Jannsen et al. (1985). With this method, we may quickly compute synthetic spectra and include all the data within a window without having first to align the phases or compute individual arrival times. Several traces are analyzed at once (Fig. 4A) by first computing a sliding spectrum; that is, the spectrum is computed about each time sample using a windowed, cosine-tapered portion of the trace. The window length, 0.064 s, is 4.8 times the period of the dominant frequency in the SCS source, and twice the length of the entire wavelet (Fig. 2). At each time sample the spectra from all twenty traces in the group are averaged and plotted horizontally, resulting in the time vs. frequency plot shown in Figure 4B.

Based on a series of these plots across the SCS profile, we chose a series of arrival times corresponding to selected events (Fig. 4C). To enhance the performance of the inversion, the events selected met several criteria. They were far enough apart in time to allow some attenuation to occur, while still maintaining as much vertical resolution as possible. They also corresponded to higher amplitude events to improve the signal to random noise ratio. Finally, the chosen events were also important for the geologic interpretation. Layer C contains the relatively reflective upper sediments rich in $CaCO_3$, layer H represents the remainder of the HSZ section from which hydrates were found or inferred, layer B contains the gassy sediments between the bottom-simulating reflector (BSR) and a possible relict BSR, and layer G spans the possibly gassy sediments below. Only the spectra observed at the selected times (Fig. 4C, black curves) were used in the inversion.

This inversion is actually an iterative forward modeling, using the technique of very fast simulated annealing (VFSA; Ingber, 1989), a well-established, robust technique for small nonlinear problems (Sen

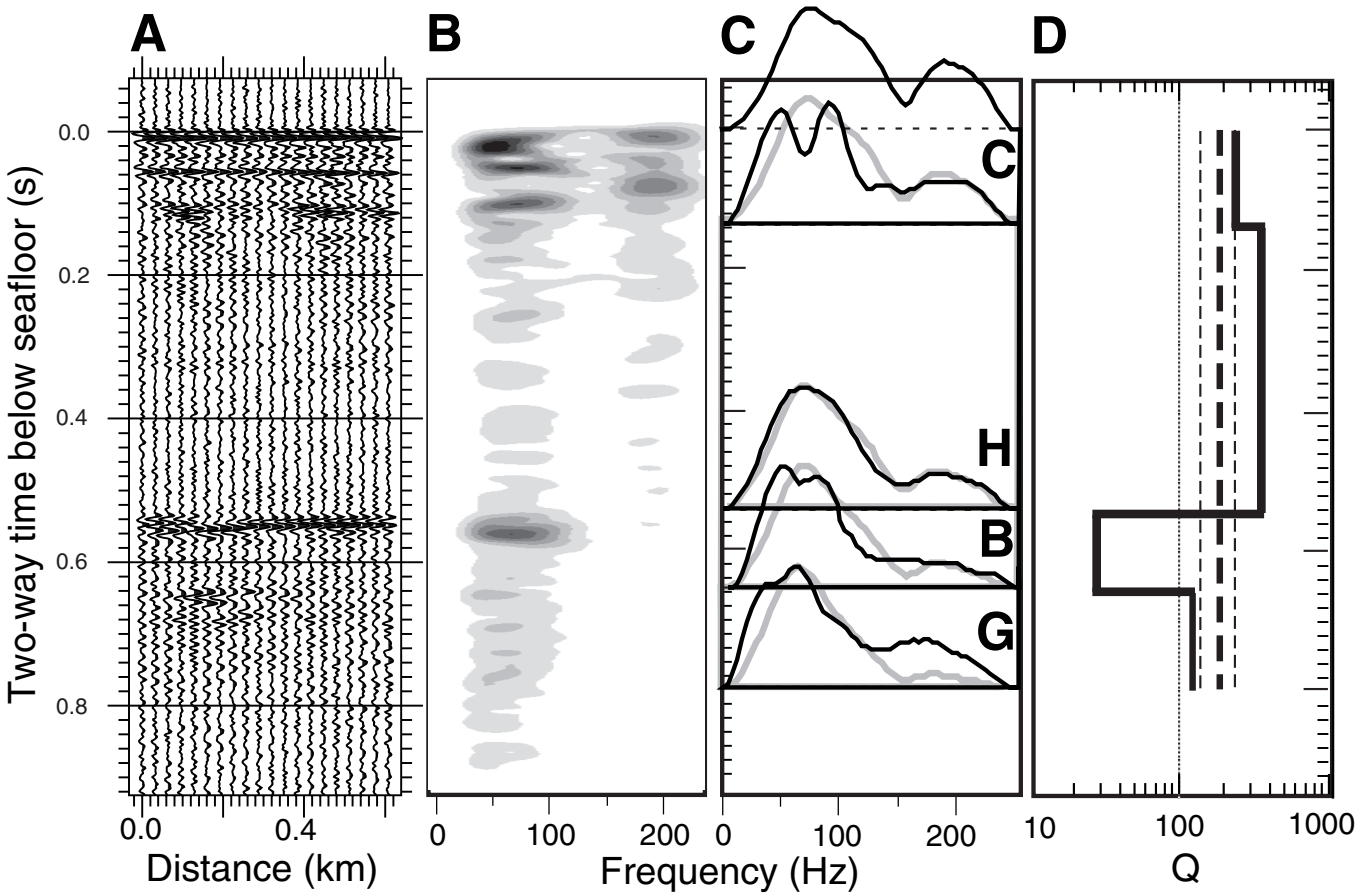

Figure 4. To invert for Q, a suite of 20 traces (**A**) is transformed into time vs. frequency (**B**; the darker shades represent higher amplitudes). (**C**) The spectra from around selected layers (dark lines) are modeled using an automated iterative forward modeling scheme (simulated annealing), resulting in a set of synthetic spectra (gray curves), and (**D**) the corresponding Q profile of the sediments (solid line). Inverting the same spectra for a constant Q yields the bold, dashed curve, with uncertainties shown as fine, dashed lines.

and Stoffa, 1991). The starting temperature and cooling rate were chosen such that convergence occurred after ~25,000 forward modelings. Although the problem may be linearized and solved much faster by working in the log spectral domain, this amplifies the noise at low points in the spectrum, resulting in a less robust comparison of synthetic and observed spectra. The forward modeling is quite fast on modern desktop computers (~15 s for 25,000 forward modelings), so speed was sacrificed and the nonlinear, but more robust, comparison was used.

The forward modeling consisted of a direct implementation of Equation 1 for each frequency as it propagates through each layer, using the spectrum at the water bottom as a reference. We assume that the selected times correspond to boundaries of homogeneous, laterally invariant layers, each of which has a constant Q. Input times are two way for reflection seismograms. For each frequency sample in the reference spectrum, an amplitude decay for each constant time thickness layer was computed using Equation 1. The decay terms were applied to each layer successively down through the section, yielding a predicted amplitude spectrum at each of the chosen interface times. The predicted spectra were individually normalized and were subtracted from the individually normalized observed spectra. The absolute value of this difference was used as the objective function; the quantity minimized by VFSA. The spectra were computed and subtracted in the linear, not log domain, and because the amplitude spectrum is independent of phase, phase computations were not needed. The objective function was computed for all layer spectra simultaneously, not sequentially (Fig. 4C, gray curves). This results in a more realistic overall solution but may also result in one layer being modeled with a slightly higher Q (high frequencies higher than observed) if a lower layer also has high-amplitude high frequencies. The Q profile that results in the minimum difference between predicted and observed spectra is taken to be the best estimate (Fig. 4D, bold).

One advantage of VFSA is that the large number of models and computed objective function values can be used to estimate the uncertainty in the final model (Sen and Stoffa, 1991). When the minimum objective function lies at the bottom of a steep-sided trough, a small change in the model corresponds to a large misfit, so the uncertainties are small. Conversely, a small change in a model corresponding to an objective function value lying at the bottom of a broad basin results in a much smaller change in misfit, so uncertainties are large. We define the uncertainty as the width of the objective function at a height of 1% from the minimum to the maximum objective function value. For the Q profile in Figure 4D, this results in an uncertainty range in Q on the order of several hundred for each layer. The uncertainty can be significantly reduced if we sacrifice vertical resolution, and invert for a single value of Q (bold, dashed line in Fig. 4D) using the same suite of observed spectra. The same 1% criterion here results in a much smaller uncertainty, as shown by the relatively narrow "error" bars on the inversion (fine, dashed lines in Fig. 4D).

RESULTS

Single-Channel Data

The results of the Q inversion described above applied to the SCS data are shown in Figure 3C. The analysis was performed on groups of 20 traces divided into four layers by five interfaces shown in Figure 3A. The time thicknesses for the selected layers remained constant across the section, and hard lower and upper bounds of $Q = 5$ and 2000 respectively were used to limit the models. Q values of 2000, adjacent to the hard bound, were assumed to be erroneous and were omitted. Values of $Q = 5$ were not encountered.

Immediately apparent in the Q profiles for each layer is that Q in the HSZ (layers C and H) is systematically higher (Q = 90–600) than in the GSZ (layers B and G, Q = 10–200). Also apparent is the gradual decrease in Q from the southwest to northeast (left to right) until a minimum is reached, after which Q increases more sharply. At Site 995, curve C is high, ~500–600, sloping downward to a minimum of 80–90 at Site 997, and rising to 150–200 at the northeast edge of the section. Although these values are not remarkably low, they may be lowered by the effects of intrabed multiples, which we expect to play a more dominant role in the layers with more reflective sediments like those in layer C.

Q for layer H nearly parallels Q for layer C, starting again at 500–600 at Site 995, but is systematically higher, reaching a minimum at 100–200, 1–2 km southwest of Site 997, and then rising very sharply back to 500–600 before reaching Site 997. Layer H is where most of the hydrates were found (and where the least reflectivity is observed) and is where we expect to find the highest values of Q. The lower two layers are known to contain some free gas and are therefore expected to exhibit lower values of Q, which the results confirm. Layer B in the GSZ starts at Q = 200–300 in the southwest and decreases to Q = 30–50 at Site 995 with a very slight increase to Q = 70–150 in the northeast. Similarly, layer G in the GSZ starts at Q = 150–250 in the southwest, decreasing sharply to near $Q = 10$ between Sites 994 and 995, rising gradually to Q = 40–60 by Site 997, and systematically showing the lowest Q of the four layers. Although the uncertainties mentioned above are larger than many of the differences we see at any given point in Figure 3C, the existence of such systematic behavior suggests that the trend across the section is more certain than the analysis at any single location.

VSPs

Although the travel times obtained from the VSPs were quite useful in delineating the V_p structure across the ridge (Holbrook et al., 1996), the actual waveform data was somewhat disappointing. Although accurate traveltime picks were obtained, an unpredictable clamping arm malfunction and a generally noisy environment significantly degraded the waveforms. Several attempts were made to identify sources of both electrical noise in the area of the underway geophysics lab and acoustic noise emanating from the hull of the drill ship (Hoskins and Wood, 1997), but little could be done to mitigate either. The cleanest displays of the time domain VSP data are shown in the *Initial Reports* volume (Paull, Matsumoto, Wallace, et al., 1996): Site 994 on p. 136, Site 995 on p. 207, and Site 997 on p. 306. To make these displays, only the clearest traces from the most powerful source (the air gun) were filtered stacked at each clamp depth. Because Site 995 was significantly less noisy than the other two sites, our efforts were concentrated on that data set.

The revised processing included editing out visibly bad traces and then time shifting the data so that the first arrivals at each clamp could easily be windowed from the rest of the trace, which was frequently quite contaminated with noise. The data were bandpass filtered, keeping only the range with the most power, 10–120 Hz. Spectra of the windowed first arrivals were computed and stacked over each clamp depth with a median stacking algorithm to mitigate the effect of outliers. Noisy spectra in the final stack were edited out leaving the display shown in Figure 5A. A similar procedure was applied to the water-gun data resulting in the display shown in Figure 5C. Unfortunately the data were too noisy to obtain Q estimates from the spectral modeling technique used on the SCS data.

Despite the noise, a significant shift in the frequency content is resolvable in the spectral data at the depth of the BSR. The effect is accentuated by the lobate nature of the spectrum, in which higher frequency lobes are more acutely bent than are the lower frequency lobes. This bending can be modeled to estimate Q. The most prominent lobe (Fig. 5B) was used to invert for a two-layer Q model (HSZ over GSZ). In the top layer, almost no frequency shift was visible. The two lines indicate the expected trajectory of this lobe in depth given a Q of 10 and 20. Clearly, any higher Q than 20 results in no shift, so we may only put a lower limit on this layer of $Q = 20$. These data are less sensitive to Q not just because of the increased noise, but primarily because of the low frequency at which the modeling is done (55 Hz vs. 200 Hz for the SCS data). Because Q for the GSZ is sig-

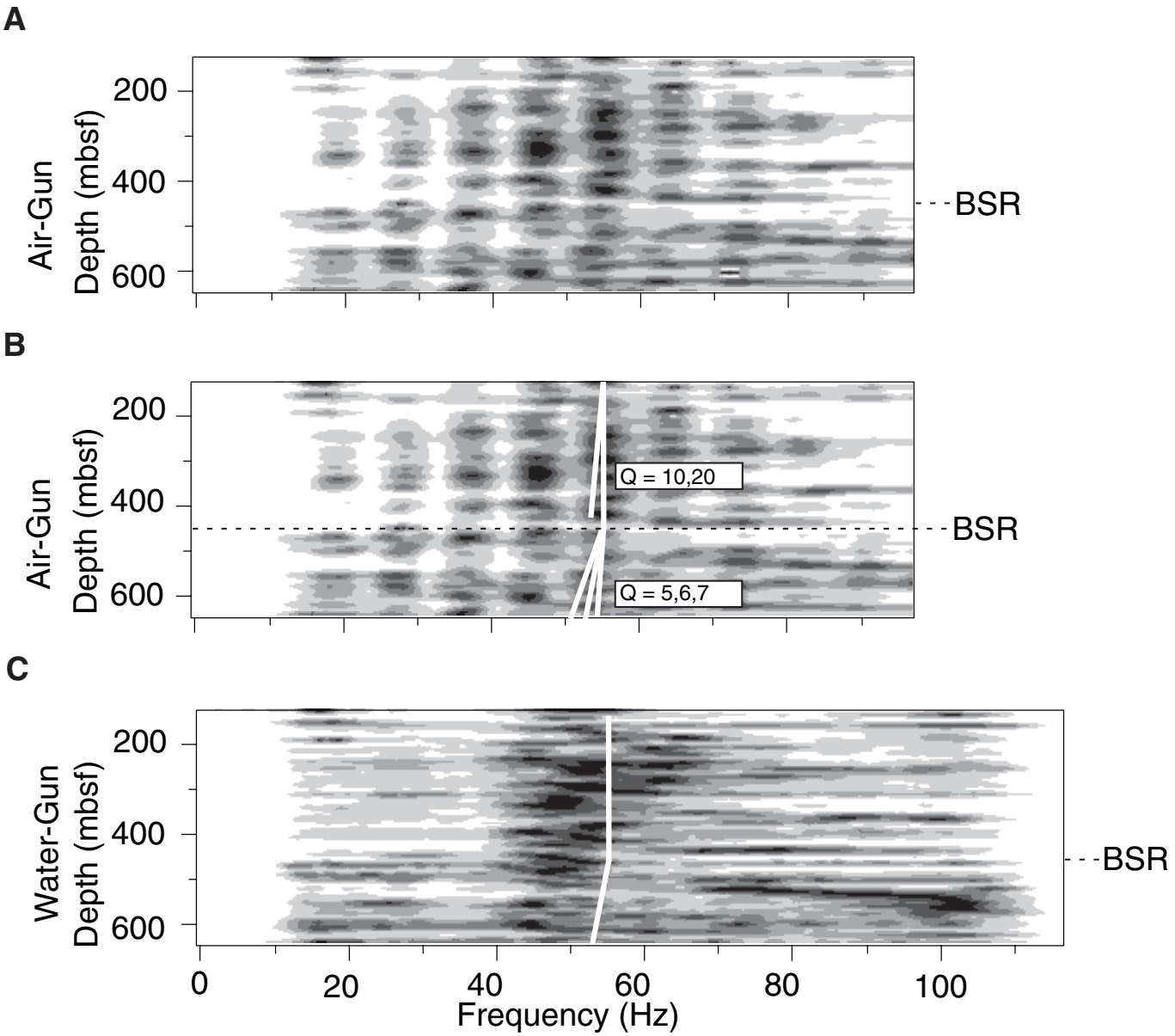

Figure 5. The spectra from the air-gun VSP (**A, B**) and water-gun VSP (**C**) data at Site 995 do not show as great a sensitivity to Q as the SCS data because of their lower frequency content and lower signal to noise ratio (darker shades represent higher amplitudes). Modeling the peak lobe of the air-gun data with a two-layer model (B) yields $Q > 10$ for the upper layer and $Q = 6$ for the lower layer. This is not inconsistent with the SCS Q inversion results or with the water-gun spectrum.

nificantly lower, we may identify Q quite readily at a value of 6; the three lines show the expected result when the upper layer is modeled with $Q = 20$ and the lower layer is modeled with $Q = 5$, 6, and 7 (Fig. 5B). The final model is drawn over the somewhat lower power water-gun data and appears to be consistent, but the water-gun spectra do not exhibit the lobate character that facilitated the previous analysis and accurate modeling is not possible.

INTERPRETATION

The behavior of Q in layers B and G in the SCS data is consistent with the reflectivity seen in the seismic data and the frequency shift seen in the spectrogram. Southwest of Site 994, the reflections between 0.55 and 0.8 s are relatively weaker than they are to the northeast and the frequency content and Q values are significantly higher. Northeast of Site 995 the reflection strengths increase as the frequencies and Q values decrease. Northeast of Site 997 there is a slight increase in frequency and Q. We know from drilling (Paull, Matsumoto, Wallace, et al., 1996) that these highly reflective layers contain significant quantities of free gas (up to 12% by volume at Site 997, [Dickens et al., 1997]), but at least the presence of gas could probably have been determined before drilling. Gas seems to be the only geologically reasonable way to explain Q as low as 10–20 in a fine-grained sediment drift. At Site 995, the results from the VSP are reasonably consistent with the SCS inversion, indicating a $Q > 20$ for the HSZ (Q = 200–300 in SCS data), and $Q = 6$ for the GSZ (Q = 10–20 in SCS data). On the basis of the scatter in the curves from the SCS data, we believe the GSZ Q estimate from the VSP is more reliable.

Determining the amount of gas from the curves in Figure 3 is somewhat more difficult. We know from a pressurized core recovery that gas occupies ~12% of the total volume near the BSR at Site 997,

where Q in the GSZ is 40–80. Although values of Q are even lower at Site 995, it is uncertain whether this is due to a higher concentration of gas, a more extensive vertical distribution of gas, or both. The latter case seems to be supported by the seismic data, where a thinner zone of stronger reflections exists at Site 997 (0.55–0.64 s) as compared to a thicker zone of only slightly weaker reflectors at Site 995 (0.55–0.8 s). The slightly, but systematically lower Q found in layer G suggests even more gas than in layer B, especially at Site 995, reinforcing the notion of a thick gas zone that elevates the reflectivity of the sediments below the BSR (Holbrook et. al, 1996). Recall also that Q may not uniquely determine the percent saturation. The data of Murphy (1982) in sandstones suggests a peak attenuation at ~90% water saturation after which attenuation decreases with decreasing water saturation. Quantification may only be possible where small quantities of gas are present or may yield a minimum estimate of the amount of gas. In either case, a more consistent means of quantifying gas in situ is required for corroboration.

The results of the Q inversion in the HSZ are more difficult to interpret than the results in the GSZ. There are no apparent lateral changes in the seismic data or spectrogram that seem to correlate to the lateral changes in Q for layers C and H. If higher values of Q were associated with higher concentrations of hydrate, we might expect more laterally consistent values, based on the relatively consistent chloride anomaly proxy (Paull, Matsumoto, Wallace, et al., 1996). Instead the minimum occurs about 2 km southwest of Site 997, directly below the ridge crest. Although the Q in layers C and H may be augmented by scattering, it is difficult to see how the scattering could change so systematically across the section. Also, if this change was some artifact of the modeling, it would likely be more closely correlated to the curves from the GSZ that appear to reach a minimum 5–7 km to the southwest.

CONCLUSIONS

As expected, the seismic Q measurements, like the V_p measurements, are shown to be more sensitive to small quantities of gas than to small quantities of hydrate. The gas-charged sediments of the Blake Ridge exhibit very low values of Q, between 6 ± 1 and 90 ± 10, significantly lower than the 200–700 range expected for fine-grained marine sediments with no gas or hydrate. Conversely, the hydrate-bearing sediments containing 3%–4% by volume hydrate exhibited values of Q between 90 ± 10 and 500 ± 100. This is slightly lower than, but generally consistent with the expected value for nonhydrate-bearing sediment.

Despite these findings we note that several authors (Brienzo, 1992; Hamilton, 1976; Jacobson et al., 1981; and Bowles, 1997) have attempted to establish a typical attenuation profile with depth, employing mechanisms such as porosity decrease with depth. The possible presence of hydrate in these areas should not yet be discounted as an agent that affects attenuation. However, this may be more pertinent to smaller spatial scale studies, where higher concentrations of hydrates may be associated with localized fluid flow.

Regarding the inversion technique, it is clear that a simple spectrogram (as shown in Fig. 3B) is adequate to detect the top of the free-gas zone. However, a full inversion for Q may be useful in remotely quantifying free-gas concentration, but only when equipment such as the pressure core sampler (Paull, Matsumoto, Wallace, et al., 1996) can be used for reliable corroboration.

ACKNOWLEDGMENTS

The authors thank the Leg 164 Scientific Party for enlightening discussions, and Graham Westbrook, Anne Trehu, Joseph Gettrust, and Sam Tooma for very helpful reviews. The work was supported by the Office of Naval Research Program Element No. 0601153N.

REFERENCES

Aki, K., and Richards, P.G., 1980. *Quantitative Seismology* (Vol. 1): New York (W. H. Freeman and Co.).

Badri, M., and Mooney, H.M., 1987. Q measurements from compressional seismic waves in unconsolidated sediments. *Geophysics,* 52:772–784.

Bowles, F.A., 1997. Observations on attenuation and shear-wave velocity in fine-grained, marine sediments. *J. Acoust. Soc. Am*., 101:3385–3397.

Brienzo, R.K., 1992. Velocity and attenuation profiles in the Monterey Deep-Sea Fan. *J. Acoust. Soc. Am*., 92:2109–2125.

Dickens, G.R., Paull, C.K., Wallace, P., and the ODP Leg 164 Scientific Party, 1997. Direct measurement of in situ methane quantities in a large gas-hydrate reservoir. *Nature,* 385:427–428.

Dvorkin, J., and Nur, A., 1993. Rock physics for characterization of gas hydrates. In *The Future of Energy Gases.* Geol. Surv. Prof. Pap. U.S., 1570.

Frisillo, A.L., and Stewart, T.J., 1980. Effect of partial gas/brine saturation on ultrasonic absorption in sandstone. *J. Geophys. Res.*, 85:5209–5211.

Gelius, L.J., 1987. Inverse Q filtering: a spectral balancing technique. *Geophys. Prospect.* 35:656–667.

Hamilton, E.L., 1976. Sound attenuation as a function of depth in the seafloor. *J. Acoust. Soc. Am.,* 59:528–535.

Hauge, P.S., 1981. Measurements of attenuation from vertical seismic profiles. *Geophysics,* 46:1548–1558.

Holbrook, W.S., Hoskins, H., Wood, W.T., Stephen, R.A., Lizzarralde, D., and the Leg 164 Science Party, 1996. Methane gas-hydrate and free gas on the Blake Ridge from vertical seismic profiling. *Science,* 273:1840–1843.

Hoskins, H., and Wood, W., 1996. Seismic acquisition system grounding and noise. *In* Paull, C.K., Matsumoto, R., Wallace, P.J., et al., *Proc. ODP, Init. Repts.,* 164: College Station, TX (Ocean Drilling Program), 43–46.

Ingber, L., 1989. Very fast simulated re-annealing. *Math. Comput. Modeling*, 12:967–973.

Jacobson, R.S., Shor, G.G., and Dorman, L.M., 1981. Linear inversion of body wave data. Part II: Attenuation vs. depth using spectral ratios. *Geophysics,* 46:152–162.

Jannsen, D., Voss, J., and Theilen, F., 1985. Comparison to determine Q in shallow marine sediments from vertical reflection seismograms. *Geophys. Prospect.*, 33:479–497.

Johnston, D.H., Toksoz, M.N., and Timur, A., 1979. Attenuation of seismic waves in dry and saturated rocks. II: Mechanisms. *Geophysics,* 44:691–711.

Kang, I.B., and McMechan, G.A., 1994. Separation of intrinsic and scattering Q based on frequency-dependent amplitude ratios of transmitted waves. *J. Geophys. Res*., 99:23875–23885.

Katzman, R., Holbrook, W.S., and Paull, C.K., 1994. A combined vertical incidence and wide-angle seismic study of a gas hydrate zone, Blake Outer Ridge. *J. Geophys. Res.,* 99:17975–17995.

Ko.renaga, J., Holbrook, W.S., Singh, S.C., and Minshull, T.A., 1997. Natural gas hydrates on the southeast U.S. margin: constraints from full waveform traveltime inversions of wide-angle seismic data. *J. Geophys. Res.*, 102:15345–15365.

LeBlanc, L.R., Panda, S., and Schock, S.G., 1991. Sonar attenuation modeling for classification for marine sediments. *J. Acoust. Soc. Am.,* 91:116–126.

Murphy, W.F., 1982. Effects of partial water saturation on attenuation in Massilon sandstone and Vycor porous glass. *J. Acoust. Soc. Am*., 71:1458–1468.

Panda, S., LeBlanc, L.R., and Schock, S.G., 1994. Sediment classification based on impedance and attenuation estimation. *J. Acoust. Soc. Am*., 96:3022–3035.

Paull, C.K., and Dillon, W.P., 1981. Appearance and distribution of the gas hydrate reflector in the Blake Ridge region, offshore southeastern United States. *USGS Misc. Field Studies Map,* 1252.

Paull, C.K., Matsumoto, R., Wallace, P.J., et al., 1996. *Proc. ODP, Init. Repts.,* 164: College Station, TX (Ocean Drilling Program).

Pecher, I.A., Holbrook, W.S., Lizarralde, D., Stephen, R.A., Hoskins, H., Hutchinson, D.R., and Wood, W.T., 1997. Shear waves through methane hydrate-bearing sediments - results from a wide angle experiment during ODP Leg 164. *Eos,* 78:F340.

Rowe, M.M., and Gettrust, J.F., 1993. Faulted structure of the bottom-simulating reflector on the Blake Ridge, western North Atlantic. *Geology,* 21:833–836.

Schoenberger, M., and Levin, F.K., 1974. Apparent attenuation due to intrabed multiples. *Geophysics,* 39:278–291.

————, 1978. Apparent attenuation due to intrabed multiples, II. *Geophysics,* 43:730–737.

Sen, M.K., and Stoffa, P.L., 1991. Nonlinear, one-dimensional seismic waveform inversion using simulated annealing. *Geophysics*, 56:1624–1638.

Stoll, R.D., and Bryan, G.M., 1970. Wave attenuation in saturated sediments. *J. Acoust. Soc. Am.*, 47:1440–1447.

Tarif, P., and Bourbie, T., 1987. Experimental comparison between spectral ratio and rise time techniques for attenuation measurements. *Geophys. Prospect.,* 35:668–680.

Toksoz, M.N., Johnston, D.H., and Timur, A., 1979. Attenuation of seismic waves in dry and saturated rock: I. Laboratory measurements. *Geophysics,* 44:681–690.

Wood, W.T., Stoffa, P.L., and Shipley, T.H., 1994. Quantitative detection of methane hydrate through high-resolution seismic velocity analysis. *J. Geophys. Res.,* 99:9681–9695.

Date of initial receipt: 15 April 1998
Date of acceptance: 10 March 1999
Ms 164SR-246